THE JOURNAL OF BIOLOGICAL CHEMISTRY VOL. 282, NO. 48, pp. 34958–34967, November 30, 2007

Stat3 Isoforms, α and β, Demonstrate Distinct Intracellular Dynamics with Prolonged Nuclear Retention of Stat3β Mapping to Its Unique C-terminal End*[S]

Received for publication, June 4, 2007, and in revised form, September 10, 2007 Published, JBC Papers in Press, September 12, 2007, DOI 10.1074/jbc.M704548200

Ying Huang[‡§], Jihui Qiu[‡], Shuo Dong[‡], Michele S. Redell[¶], Valeria Poli[‖], Michael A. Mancini[**], and David J. Tweardy[‡1]**

*From the [‡]Department of Medicine, Section of Infectious Diseases, [¶]Department of Pediatrics, Section of Hematology/Oncology, and **Department of Molecular and Cellular Biology, Baylor College of Medicine, Houston, Texas 77030, the [§]Department of Pathophysiology, Key Laboratory of Cell Differentiation and Apoptosis of the Chinese Ministry of Education, Shanghai Jiao Tong University School of Medicine, Shanghai, China, and the [‖]Departments of Genetics, Biology, and Biochemistry, University of Turin, Via Nizza 52, Turin 10126, Italy*

Two isoforms of Stat3 (signal transducer and activator of transcription 3) are expressed in cells, α (p92) and β (p83), both derived from a single gene by alternative mRNA splicing. The 55-residue C-terminal transactivation domain of Stat3α is deleted in Stat3β and replaced by seven unique C-terminal residues (CT7) whose function remains uncertain. We subcloned the open reading frames of Stat3α and Stat3β into the C terminus of green fluorescent protein (GFP). Fluorescent microscopic analysis of HEK293T cells transiently transfected with GFP-Stat3α or GFP-Stat3β revealed similar kinetics and cytokine concentration dependence of nuclear accumulation; these findings were confirmed by high throughput microscope analysis of murine embryonic fibroblasts that lacked endogenous Stat3 but stably expressed either GFP-Stat3α or GFP-Stat3β. However, although time to half-maximal cytoplasmic reaccumulation after cytokine withdrawal was 15 min for GFP-Stat3α, it was >180 min for GFP-Stat3β. Furthermore, although the intranuclear mobility of GFP-Stat3α was rapid and increased with cytokine stimulation, the intranuclear mobility of GFP-Stat3β in unstimulated cells was slower than that of GFP-Stat3α in unstimulated cells and was slowed further following cytokine stimulation. Deletion of the unique CT7 domain from Stat3β eliminated prolonged nuclear retention but did not alter its intranuclear mobility. Thus, Stat3α and Stat3β have distinct intracellular dynamics, with Stat3β exhibiting prolonged nuclear retention and reduced intranuclear mobility especially following ligand stimulation. Prolonged nuclear retention, but not reduced intranuclear mobility, mapped to the CT7 domain of Stat3β.

There are seven members of the signal transducer and activator of transcription (STAT)[2] family of latent transcription factors (1, 2, 3, 4, 5A, 5B, and 6), each initially identified within cytokine and growth factor signaling pathways downstream of Jak or intrinsic receptor tyrosine kinases (1). Stat3, originally known as acute phase response factor, was identified (2) and cloned within the interleukin (IL)-6 pathway (3) and by low stringency cDNA homology screening (4). Isoforms of STAT proteins generated by alternative mRNA splicing have been demonstrated for Stat1 (5), Stat3 (6–8), Stat4 (9), Stat5A (10), Stat5B (11), and Stat6 (12). In each instance, the isoforms are derived from a single gene transcript by alternative splicing. In addition, isoforms of Stat3, Stat5A, Stat5B, and Stat6 have been identified that result from proteolytic cleavage (13–20). Most isoforms generated by alternative splicing or proteolysis are C-terminal truncation mutants that act as dominant negatives of their full-length counterparts by virtue of missing the C-terminal transactivation domain. In the case of Stat3β, however, the 55-amino acid C-terminal acidic transactivation domain of Stat3α is replaced by seven unique amino acid residues (CT7 domain).

Stat3β was isolated initially in the mouse using a yeast two-hybrid strategy with the N terminus of c-Jun as bait (6). The CT7 domain was presumed responsible for this interaction; however, subsequent studies revealed that residues within the coiled-coil and DNA binding domains of Stat3, common to both isoforms, were found to be responsible for c-Jun interaction, thereby leaving unresolved the functional role of the CT7 domain if any.

To gain additional insight into the unique aspects of Stat3β at the single cell level and how the CT7 domain may contribute to them, we subcloned the open reading frames of Stat3α and Stat3β into the C terminus of GFP and transfected them into HEK293T and mouse embryo fibroblast (MEF) cells; endogenous Stat3α and Stat3β were deleted within MEF cells

* This work was supported in part by National Institutes of Health Grant CA72261. The costs of publication of this article were defrayed in part by the payment of page charges. This article must therefore be hereby marked "*advertisement*" in accordance with 18 U.S.C. Section 1734 solely to indicate this fact.

[S] The on-line version of this article (available at http://www.jbc.org) contains supplemental Fig. 1.

[1] To whom correspondence should be addressed: Section of Infectious Diseases, Dept. of Medicine, Baylor College of Medicine, One Baylor Plaza, BCM 286, Rm. N1319, Houston, TX 77030. Tel.: 713-798-8918; Fax: 713-798-8948; E-mail: dtweardy@bcm.edu.

[2] The abbreviations used are: STAT, signal transducer and activator of transcription; IL, interleukin; CT7, seven unique C-terminal residues; MEF, mouse embryo fibroblast; sIL-6R, soluble IL-6 receptor; G-CSF, granulocyte colony-stimulating factor; G-CSFR, G-CSF receptor; GFP, green fluorescent protein; PIPES, 1,4-piperazinediethanesulfonic acid; HTM, high throughput microscope; FLIN, fractional localized intensity in the nucleus; FRAP, fluorescence recovery after photobleaching.

using Cre-lox technology. Cytokine stimulation of the resultant cell lines revealed similar kinetics of nuclear accumulation for GFP-Stat3α and GFP-Stat3β. However, cytoplasmic reaccumulation after ligand removal, although rapid for GFP-Stat3α ($t_{½}$ = 15 min), was markedly delayed for GFP-Stat3β ($t_{½}$ > 180 min). Prolonged nuclear retention of Stat3β was accompanied by reduced intranuclear mobility and increased immobile fraction. Interestingly, prolonged nuclear retention but neither reduced intranuclear mobility nor increased immobile fraction mapped to the CT7 domain of Stat3β.

EXPERIMENTAL PROCEDURES

Cell Lines and Cytokines—The human embryonic kidney fibroblast cell line HEK293T and the human hepatoma cell line HepG2 were cultured in Dulbecco's modified Eagle's medium (Invitrogen) with 10% fetal bovine serum, penicillin (100 units/ml) and streptomycin (100 units/ml). HeLa cells were grown in Opti-MEM I medium (Invitrogen) with 4% fetal bovine serum. $Stat3^{\Delta/\Delta}$ MEFs and $Stat3^{fl/fl}$ MEF kindly provided by Dr. Valeria Poli (University of Turin, Italy) (21) were cultured in 10% DMEM with 10% fetal bovine serum, 1× amino acids, penicillin (100 units/ml), and streptomycin (100 units/ml). Human IL-6 and soluble IL-6 receptor (sIL-6R) were purchased from R & D Systems (Minneapolis, MN). Human G-CSF was purchased from Santa Cruz Biotechnology, Inc. (Santa Cruz, CA).

Plasmid—GFP-Stat3α and GFP-Stat3β expression vectors were constructed by subcloning the full-length cDNA of human Stat3α and Stat3β in frame 3′ of GFP contained within pEGFP-C1 (Clontech) using the appropriate enzyme digestion fragments. The truncated Stat3β mutant construct (deletion of the C-terminal 7 amino acids; Stat3βΔ) was generated by substituting a stop codon for that encoding the first in the 7-amino acid sequence using QuikChange II site-directed mutagenesis kit (Stratagene). All constructs were confirmed by DNA sequencing. An acute phase response element (APRE)-luciferase reporter construct, which has four copies of APREs, was kindly provided by Dr. I. Matsumura (Osaka, Japan). The full-length G-CSF receptor cDNA was obtained and used as described previously (22).

Luciferase Assay—For transient transfections, MEFs were grown in 6-well (35-mm diameter) tissue culture plates to 50–70% confluence. Twelve hours later, the cells were transiently transfected with the indicated expression vectors and reporter genes using the GeneJuice transfection reagents according to the manufacturer's instruction as previously reported (23). The amounts of plasmid DNA used per well were 250 ng of reporter vector, 1 μg of expression vector, and 250 ng of β-galactosidase expression vector (Promega, Madison, WI) as transfection control. Luciferase activity was measured in a luminometer (Luminoskan Ascent, Labsystems, Franklin, MA), expressed in arbitrary units, and normalized according to the transcriptional efficiency from β-galactosidase expression. Each point is the mean of at least three independent experiments.

Gel Shift Assay—HEK293T cells were transiently transfected in 6-well plates using 2 μg of plasmid. Forty-eight hours later, cells were either not treated or treated for 30 min with G-CSF (100 ng/ml). Whole cell extracts were prepared, and gel shift assays were performed as described previously (23). Briefly, 20 μg of whole cell extract protein was incubated with [γ-^{32}P]adenosine triphosphate (ATP; PerkinElmer Life Sciences) end-labeled duplex oligonucleotide high affinity serum-inducible element probe at 37 °C for 2 h in the following binding buffer: 20 mM Hepes, pH 7.4, 50 mM KCl, 1 mM 2-mercaptoethanol, 10% glycerol, 1 μg of poly(dI-dC) (Amersham Biosciences), and 100 μg of bovine serum albumin. Protein-DNA complexes were separated on 4.5% polyacrylamide gels equilibrated in 0.25× Tris borate-EDTA buffer (TBE). Gels were dried and exposed to PhosphorImager plates, and images were developed and quantitated using a PhosphorImager (Amersham Biosciences) and ImageQuant software.

Immunoblotting—Whole cell lysates were prepared in lysis buffer (20 mM Hepes, pH 7.9, 420 mM NaCl, 20 mM NaF, 1 mM Na_3VO_4, 1 mM $Na_4P_2O_7$, 1 mM EDTA, 1 mM EGTA, 1 mM dithiothreitol, 20% glycerol, 0.5 mM phenylmethylsulfonyl fluoride). Equivalent amounts of total cellular protein were electrophoresed on 7.5% SDS-polyacrylamide gel and transferred to polyvinylidene difluoride membrane (Millipore). Probing of polyvinylidene difluoride membranes with primary antibodies and detection of horseradish peroxidase-conjugated secondary antibodies by enhanced chemiluminescence was as indicated (Amersham Biosciences). Antibodies used in this study were as follows: Stat3 monoclonal antibody obtained from Transduction Laboratories (Lexington, KY) and β-actin monoclonal antibody obtained from Abcam Inc.

Generation of MEF Cells Stably Expressing GFP-Stat3α or GFP-Stat3β—$Stat3^{\Delta/\Delta}$ MEFs were transfected with GFP-Stat3α or GFP-Stat3β constructs (3 μg) using DNA carrier GeneJuice reagent as reported previously (23). After transfection overnight, the cells were fed with fresh medium and incubated for 24 h. Forty-eight hours after transfection, cells were split and cultured in selection medium containing G418 (1 mg/ml; Invitrogen) at different cell concentrations to promote growth of isolated colonies. After 10 days, 50 isolated colonies of GFP-Stat3α and GFP-Stat3β were harvested using sterile cloning discs (PGC Scientific Corp.) with trypsin-EDTA (Invitrogen); each colony was replated into a single well of a 24-well plate. After 3 weeks of growth in G418-containing medium, each colony was screened for GFP expression by fluorescence microscopy. Several colonies were expanded, analyzed, and sorted for low and uniform levels of GFP expression by the Beckman Altra cell sorter. Sorted cells with levels of GFP-Stat3 isoform expression similar to endogenous levels in $Stat3^{fl/fl}$ MEF cells (Fig. 3) were selected for further analysis. MEF/GFP-Stat3βΔ cells were generated in a similar fashion with the exception that after selection in G418, cells were sorted four times to obtain cells with low and uniform levels of expression that on immunoblot analysis were similar to endogenous Stat3 levels in $Stat3^{fl/fl}$ MEF cells (Fig. 3).

High Throughput Microscope Analysis—After plating into coverslip-containing wells and incubation for 24 h, MEF/GFR-Stat3α, -β, and -βΔ cells at 75–85% confluence were incubated without or with IL-6/sIL-6Rα, fixed in 4% formaldehyde in PEM Buffer (80 mM potassium PIPES, pH 6.8, 5 mM EGTA, pH 7.0, 2 mM $MgCl_2$) for 30 min at 4 °C, quenched in 1 mg/ml $NaBH_4$ (Sigma) in PEM buffer, counterstained for 1 min in 4′,6-

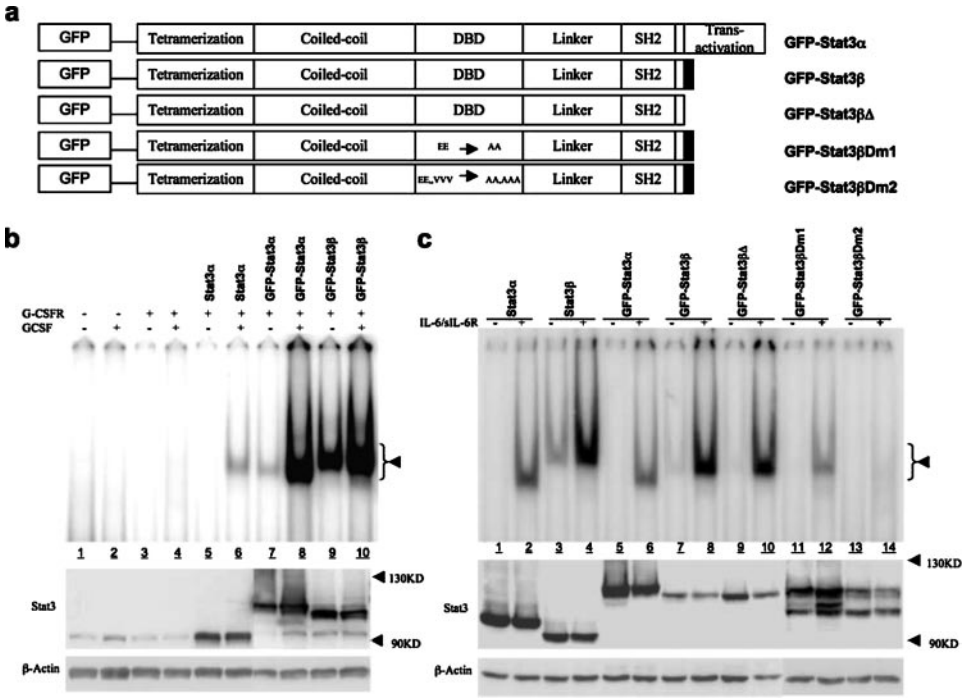

FIGURE 1. **Molecular weight and DNA binding activities of GFP-tagged wild type and mutated Stat3α and Stat3β constructs.** *a*, schematic depiction of constructs with the domains indicated, including the DNA binding domain (*DBD*) and the CT7 domain of Stat3β (*black box*). Stat3β mutants Stat3β Dm1 and Stat3β Dm2 were generated by site-directed mutagenesis at residues 434–435 and 461–463 within the DNA binding domain as indicated. *b* and *c*, gel shift assays (*top*) were performed using radiolabeled high affinity serum-inducible element and whole cell extracts of HEK293T cells co-transfected with G-CSFR and GFP-Stat3 constructs and treated with or without G-CSF (100 ng/ml) for 30 min as indicated (*b*) or of HEK293T cells co-transfected with GFP-Stat3 constructs and treated with or without IL-6 (200 ng/ml) and soluble IL-6R (250 ng/ml) (*c*). The *black arrowhead* indicates the position of the band corresponding to a high affinity serum-inducible element bound by Stat3-containing construct. In the *bottom two panels*, the extracts were immunoblotted with Stat3 antibody and β-actin antibody as indicated. The *black arrowheads* mark the positions of the indicated molecular weight markers.

diamidino-2-phenylindole (Sigma) (1 mg/ml in PEM buffer), and mounted in Slow Fade reagent (Molecular Probes).

A Beckman/Q3DM IC-100 high throughput microscope (HTM) was used to automate fluorescent image acquisition and analysis of the nuclear translocation, as described (24). The system was used to scan multiple fields and to acquire and analyze each of the cells in the images. Algorithms were generated to determine fractional localized intensity in the nucleus (FLIN) for each set of cell images, as described (25). Nuclear masks were generated by applying a nonlinear least-squares optimized image filter to create marked object-background fluorescence corrected by estimating and subtracting the mean background image intensity. The correlated channel mask was computed as an intersection between the threshold-correlated channel image (the threshold level is dynamically computed using a proprietary background level estimation method) and a circle of user-defined radius from the nuclear centroid. Different gates (area, wiggle, and absolute) were set to measure the majority of cells and to avoid overexpression or lower expression level cells and very large or small cells. The same settings were used for examining FLIN in all experiments.

Fluorescence Recovery after Photobleaching—Prior to live cell imaging, MEF/GFR-Stat3α, -β, and -βΔ cells (2×10^5 cells/dish) were incubated in 23-mm glass bottom Delta T plates (Bioptechs Inc.) until 80–90% confluent. After culturing for 24 h and treatment without and with IL-6 (200 ng/ml) and sIL-6R (250 ng/ml) for 30 min, cells were examined using an LSM 510 confocal microscope (Carl Zeiss) equipped with a 63× (numerical aperture 1.4) objective. Cells were maintained at 37 °C using a Bioptechs Delta Controller, and fresh medium without or with IL-6 and sIL-6R was cycled over the cells. Five single imaging scans were acquired prior to bleaching. A bleach pulse of 2 s was delivered using a 488-nm laser set for GFP maximum power for 20 iterations (laser output, 75%); immediately after the bleach, the intensity remaining was 40–50% of the original fluorescence. A single *z* section was imaged before and at time intervals following the bleach. Fluorescence intensity of the region of interest was determined using LSM software. Data were exported to Excel for analysis as previously described (26). LSM images were exported as TIF files. All of the quantitative data for fluorescence recovery after photobleaching (FRAP) recovery kinetics represent means ± S.D. from at least 18 cells imaged in two independent experiments. The immobile fraction for each cell analyzed was calculated by subtracting the mean of the last 10 single image scans from the mean of the prebleach single image scans and then dividing this value by the mean of the prebleach single image scans and multiplying by 100.

Statistical Analysis—Unless indicated otherwise, data presented are the mean ± S.E.; differences between means were assessed for significance using analysis of variance or Student's *t* test, where appropriate.

RESULTS

The Addition of GFP to the N Terminus of Stat3α or Stat3β Does Not Change Its DNA Binding or Transcriptional Activity—To study the cellular dynamics of Stat3α and Stat3β at the single cell level, the open reading frames for each were inserted into the C terminus of GFP (Fig. 1). Transient transfection of these constructs into HEK293T cells revealed expression of proteins of the anticipated size (Fig. 1) that bound DNA with activity similar to their untagged counterparts upon activation with two cytokine/receptor systems known to activate Stat3, G-CSF/G-CSFR (Fig. 1*b*) and IL-6/IL-6R (Fig. 1*c*). As shown previously for their untagged counterparts (27, 28), GFP-Stat3β displayed a higher level of DNA binding without and with cytokine/receptor addition than GFP-Stat3α.

To further characterize the functional properties of GFP-Stat3α and GFP-Stat3β compared with their untagged counterparts, we examined their transcriptional activity by luciferase reporter assay in MEF/Stat3$^{\Delta/\Delta}$ cells in which the endogenous Stat3 gene had been deleted using Cre-lox technology (21). MEF/Stat3$^{\Delta/\Delta}$ cells were co-transfected with G-CSFR, a luciferase reporter construct containing four copies of the APRE from the rat α_2-macroglobulin promoter and Stat3α, Stat3β, or both expression plasmids and treated without or with G-CSF. G-CSF-induced activation of the APRE-luciferase reporter was observed in MEF/Stat3$^{\Delta/\Delta}$ cells co-transfected with Stat3α but not in cells co-transfected with Stat3β (Fig. 2*a*), similar to results obtained by others using similar reporter constructs in COS-7 cells (8, 29). Furthermore, Stat3α-mediated activation of this reporter was inhibited by about 65% in cells co-transfected with Stat3β (Fig. 2*a*), similar to findings using reporter constructs containing the pIRE contained within the ICAM-1 promoter (8). Experiments using GFP-tagged Stat3 isoforms completely recapitulated these findings (Fig. 2*b*). Thus, the GFP tag did not alter the DNA binding or transcription activities of Stat3α and Stat3β in MEF cells.

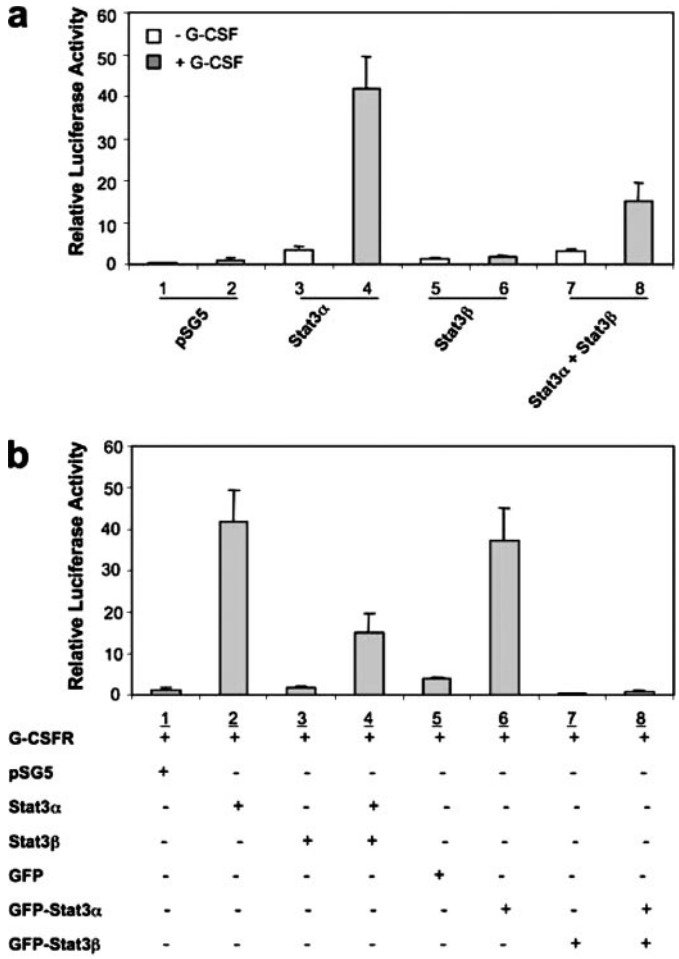

FIGURE 2. **Transcriptional activity of GFP-Stat3α and GFP-Stat3β constructs induced by G-CSF.** *a* and *b*, MEF/Stat3$^{\Delta/\Delta}$ cells were transiently co-transfected with control (pSG5) or Stat3 isoform-containing vectors along with the G-CSFR construct, the β-galactosidase expression construct and 4× APRE-luciferase reporter construct then treated with or without G-CSF (50 ng/ml) for 20 h as indicated. Luciferase activity was measured in a luminometer, expressed in arbitrary units, and normalized for the transfection efficiency by the β-galactosidase assay. The results shown represent the means ± S.E. of three separate experiments.

Examination of Nuclear Accumulation and Cytoplasmic Reaccumulation of Stat3α and Stat3β—Stat3α has been demonstrated to shuttle continuously between the cytoplasm and nucleus in unstimulated cells (30–38) and to accumulate in the nucleus following cytokine stimulation due to decreased nuclear export (30); the dynamics of Stat3β at the single cell level and how it compares to Stat3α has not been examined. To address this, we transiently co-transfected HEK293T cells with plasmids containing G-CSFR and either GFP-Stat3α or GFP-Stat3β and examined 30–50 cells by fluorescent microscopy before and after incubation with G-CSF (0, 1, 3, 10, 30, and 100 ng/ml) for 30 min (Table 1). The percentage of cells transfected with GFP-Stat3α that demonstrated predominantly nuclear localization increased from 4% cells incubated without G-CSF to 90% of cells incubated with G-CSF at 100 ng/ml; similar results were obtained at each corresponding concentrations of G-CSF for cells transfected with GFP-Stat3β. To assess the kinetics of nuclear translocation of GFP-Stat3α *versus* GFP-Stat3β, HEK293T cells co-transfected with G-CSFR and GFP-Stat3α or GFP-Stat3β were incubated without or with G-CSF (100 ng/ml) for 0, 1, 3, 10, 30, and 100 min. The percentage of cells transfected with GFP-Stat3α that demonstrated predominantly nuclear localization increased from 4% of cells at time 0 to 95% of cells at both 30 and 100 min; similar results were obtained at corresponding time points examined for cells transfected with GFP-Stat3β.

To confirm and extend these findings in cells that express only GFP-tagged Stat3α or Stat3β at levels similar to endogenous levels, MEF/Stat3$^{\Delta/\Delta}$ cells were stably transfected with the GFP-Stat3α or GFP-Stat3β plasmid constructs, and surviving colonies were sorted to obtain >90% GFP-positive cells that express GFP-Stat3 at low to moderate levels. Immunoblot analysis of representative colonies established that levels of GFP-

TABLE 1
Dose response and kinetics of nuclear accumulation of Stat3α and Stat3β following transient transfection into HEK293T cells

	Cell with predominantly nuclear accumulation[a]											
	[G-CSF][b]						Time[c]					
	0 ng/ml	1 ng/ml	3 ng/ml	10 ng/ml	30 ng/ml	100 ng/ml	0 min	1 min	3 min	10 min	30 min	100 min
	%	%	%	%	%	%	%	%	%	%	%	%
GFP-Stat3α	4	8	8	10	40	90	4	5	5	90	95	98
GFP-Stat3β	10	5	10	10	40	90	10	10	10	87	95	95

[a] 30–50 cells examined per condition.
[b] Cells incubated for 30 min.
[c] [G-CSF] = 100 ng/ml.

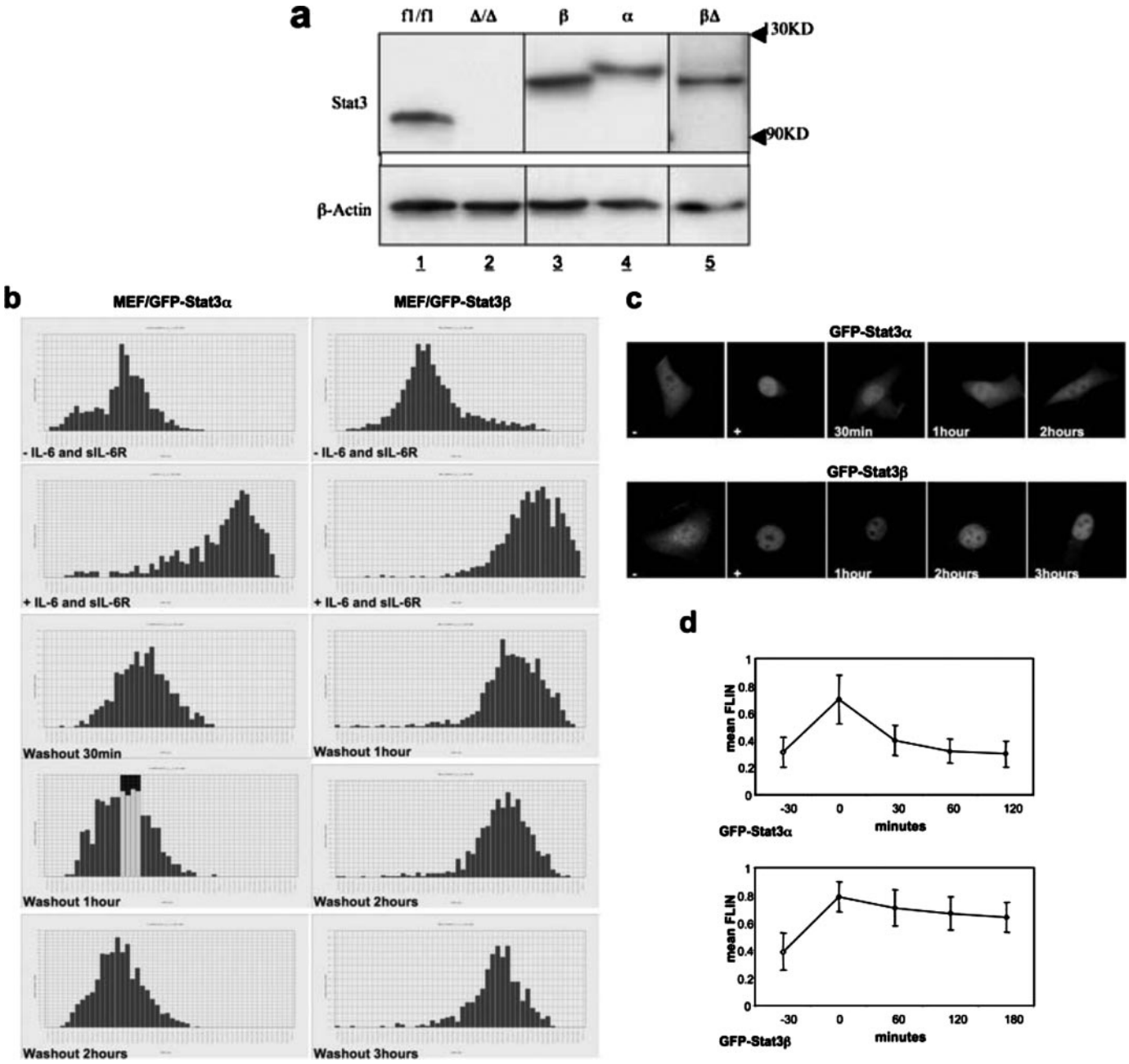

FIGURE 3. **Immunoblot and HTM analysis of MEF cell lines.** *a*, extracts of MEF/Stat3$^{fl/fl}$ (fl/fl) MEF/Stat3$^{\Delta/\Delta}$ (Δ/Δ) MEF/GFP-Stat3α (α) MEF/GFP-Stat3β (β) or MEF/GFP-Stat3βΔ (βΔ) cells were immunoblotted with monoclonal antibody against Stat3 (*top*) or β-actin (*bottom*). The *black arrowheads* mark the location of the indicated molecular weight markers. *b*, MEF/GFP-Stat3α and MEF/GFP-Stat3β cells were incubated without or with IL-6 (200 ng/ml) and sIL-6R (250 ng/ml) followed by IL-6/sIL-6R washout and incubation in medium alone for the time indicated. Cells were examined by HTM and assayed for fluorescent intensity in the nucleus (*FLIN*). Histograms show the number of cells with FLIN values ranging from 0 to 1.0 in increments of 0.02. *c*, representative fluorescent micrographs of cells are shown. *d*, mean ± S.D. of histogram results are plotted as a function of time before or after IL-6/sIL-6R washout.

Stat3α and GFP-Stat3β protein expression were similar to wild type MEF (MEF$^{fl/fl}$; Fig. 3). HTM of MEF/GFP-Stat3α and MEF/GFP-Stat3β cells (300–500 cells/condition) (Fig. 3, *b–d*) revealed similar increases in FLIN levels from 0.31 ± 0.11 for Stat3α and 0.39 ± 0.13 for Stat3β, respectively, in unstimulated cells to 0.7 ± 0.18 for α and 0.79 ± 0.11 for β, respectively, in stimulated cells. The GFP signal was distributed diffusely throughout the cytoplasm and nucleus in unstimulated MEF/GFP-Stat3α cells and predominantly within the nucleus in a diffuse pattern sparing the nucleolus in stimulated MEF/GFP-Stat3α cells, which was identical to the pattern and distribution of GFP signal in unstimulated and stimulated MEF/GFP-Stat3β cells, respectively.

To examine the kinetics of cytoplasmic reaccumulation of Stat3 isoforms, cells were removed from IL-6/sIL-6R and examined by HTM at 30–60-min intervals (Fig. 3). FLIN decreased rapidly in MEF/GFP-Stat3α cells following cytokine/receptor removal, returning to unstimulated levels within 30 min and demonstrated a time to half-maximal cytoplasmic reaccumulation ($t_{1/2}$) of 15 min. In contrast,

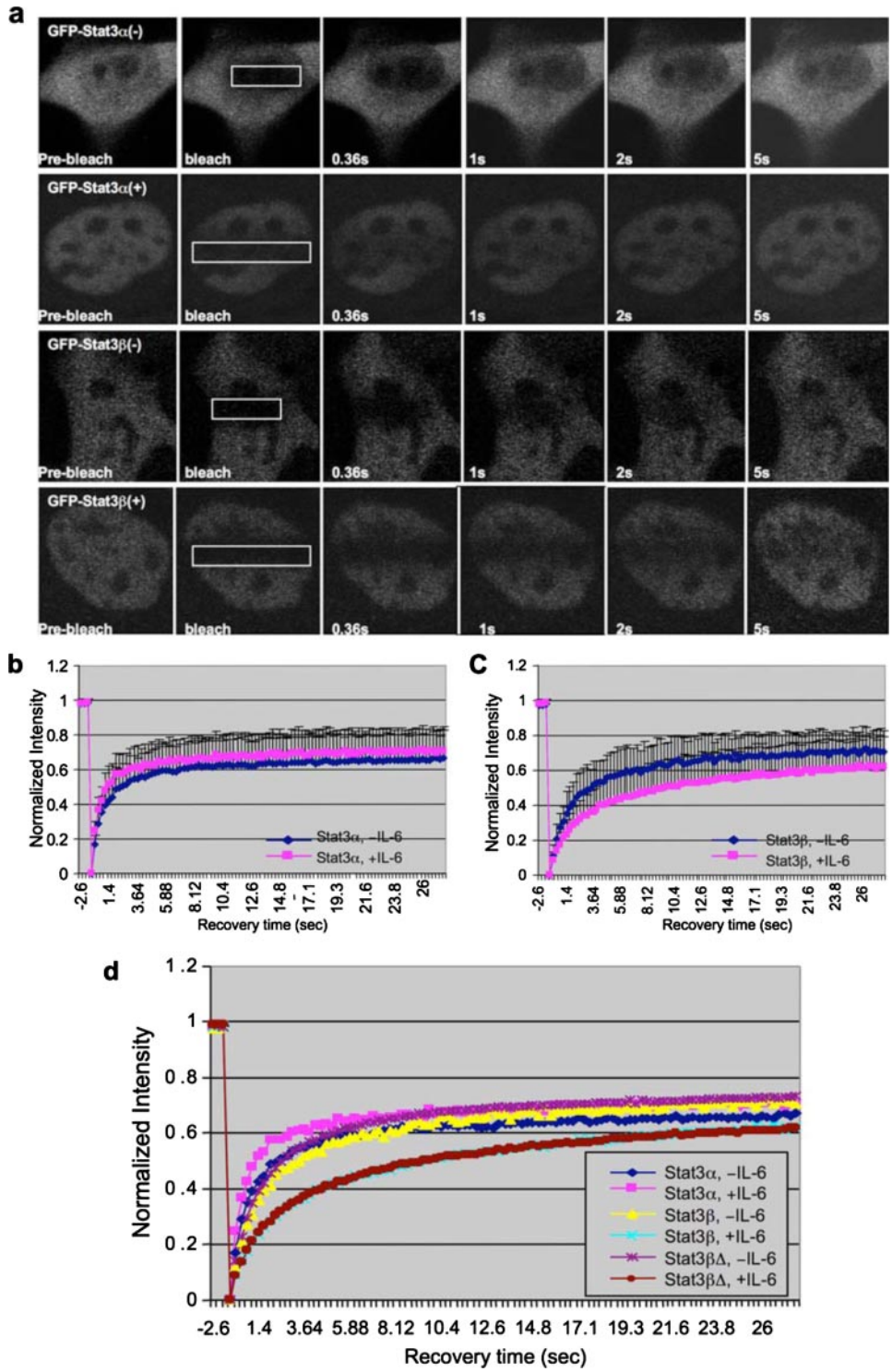

FIGURE 4. **FRAP analysis of MEF cell lines.** MEF/GFP-Stat3α and MEF/GFP-Stat3β cells were incubated without (−) or with (+) IL-6 (200 ng/ml) and sIL-6R (250 ng/ml). *a*, representative images showing a single *z* section obtained before photobleaching (*Pre-bleach*), at the end of photobleaching (*bleach*), and at the indicated time points after photobleaching. The *white rectangle* represents the area bleached within the nucleus. *b* and *c*, representative recovery curves obtained from FRAP analysis of cells are shown. The initial fluorescence for each cell was assigned a value of 1; fluorescence immediately after bleach was assigned a value of 0. Data shown are the mean ± S.D. of 20–22 cells. Each experiment was repeated at least three times with similar results. *d*, FRAP recovery curves (mean values only) from each of the relevant MEF cell lines studies were overlaid.

Examination of the Nuclear Mobility of Stat3α and Stat3β—We have previously demonstrated that aberrant nuclear sequestration of chimeric RARα-containing transcription factors found in acute promyelocytic leukemia cells is associated with their reduced nuclear mobility (26). To determine if reduced mobility of Stat3β may contribute to its nuclear retention, we performed FRAP using MEF/GFP-Stat3α and MEF/GFP-Stat3β cells (Fig. 4 and Table 2). Only cells expressing low levels of protein were examined by FRAP to avoid artifacts of overexpression as previously described (31).

The nuclear mobility of GFP-Stat3α assessed by time to half-maximal fluorescence recovery ($t_{1/2}$) was 1.01 ± 0.53 s before stimulation and increased 42% with IL-6/sIL-6R stimulation ($t_{1/2}$ = 0.59 ± 0.24 s; $p < 0.05$). The mobility of GFP-Stat3β in unstimulated cells (2.14 ± 0.83 s) was 112% slower than GFP-Stat3α in unstimulated cells ($p < 0.05$) and was slowed 48% further following IL-6/sIL-6R simulation (3.17 ± 0.71 s; $p < 0.05$).

Release from a large aggregate or complex could explain the ligand-stimulated increase in mobility of Stat3α and would be accompanied by an decrease in the immobile fraction (32). Conversely, formation of an aggregate or binding to a large complex could explain the ligand-mediated decrease in mobility of Stat3β and would be accompanied by an increased immobile fraction. Consistent with these predictions (Fig. 4 and Table 2), ligand/receptor stimulation of MEF/GFP-Stat3α cells resulted in a 13% decrease in the immobile fraction of Stat3α. In contrast, ligand stimulation of MEF/GFP-Stat3β cells resulted in a 32% increase in the immobile fraction of Stat3β. Thus, in addition to prolonged nuclear retention, Stat3β exhibited reduced nuclear mobility in both unstimulated and stimulated cells. Furthermore, in contrast to Stat3α, the mobility of Stat3β decreased and the immobile fraction increased with activation. These results are consistent with the hypothesis that reduced intranuclear mobility, accom-

FLIN of MEF/GFP-Stat3β cells decreased only slightly after cytokine/receptor removal and demonstrated a cytoplasmic reaccumulation $t_{1/2}$ of >180 min.

panied by increased immobile fraction, may contribute to prolonged nuclear retention of Stat3β.

The C-terminal 7-Amino Acid Domain of Stat3β Is Responsible for Prolonged Nuclear Retention but Not Reduced Nuclear Mobility or Increased Immobile Fraction—To determine the contribution of the CT7 domain of Stat3β to prolonged nuclear retention, reduced nuclear mobility, and increased immobile fraction, we used MEF/Stat3$^{\Delta/\Delta}$ cells to generate cells that stably express GFP-labeled Stat3β in which the CT7 domain was deleted (MEF/GFP-Stat3βΔ) (Fig. 5). Gel shift assays demonstrated that GFP-Stat3βΔ bound DNA with affinity similar to GFP-Stat3β (Fig. 1*c*, *lanes 7–10*), consistent with previous reports examining this Stat3 construct untagged with GFP (33). HTM analysis revealed that FLIN values of MEF/GFP-Stat3βΔ cells before and after stimulation with IL-6/sIL-6Rα were similar to MEF/GFP-Stat3β cells (Fig. 5). However, FLIN in MEF/GFP-Stat3βΔ cells returned to unstimulated levels within 30 min following cytokine/receptor removal with a cytoplasmic reaccumulation $t_{½}$ of 15 min, similar to GFP-Stat3α. These results indicate that the CT7 domain is responsible for prolonged nuclear retention of Stat3β. In contrast, FRAP results showed that GFP-Stat3βΔ retained mobility features of Stat3β, including reduced mobility in unstimulated cells (FRAP $t_{½}$ = 1.42 ± 0.40 s) and the property of further reduced mobility in stimulated cells (FRAP $t_{½}$ = 2.89 ± 0.67 s; $p < 0.05$). In addition, similar to Stat3β, the immobile fraction of Stat3βΔ also increased 43% with ligand stimulation (Fig. 5 and Table 2). These results indicate that although the CT7 domain is responsible for prolonged nuclear retention of Stat3β, it is not responsible for its reduced intranuclear mobility or increased immobile fraction. Furthermore, these findings suggest that reduced intranuclear mobility and increased immobile fraction do not contribute to prolonged nuclear retention; rather, the mechanism of prolonged nuclear retention is mediated through a distinct mechanism involving the CT7 domain.

TABLE 2
Summary of FRAP studies

Construct	IL-6/IL-6R	Time to half-maximal recovery ($t_{½}$) (mean ± S.E.)	Immobile fraction (mean ± S.E.)	Number of cells examined
		s	%	
GFP-Stat3α	−	1.01 ± 0.53^{a,b,c}	34.1 ± 14.6	22
	+	0.59 ± 0.24^{a,d,e}	29.6 ± 13.1	20
GFP-Stat3β	−	2.14 ± 0.83^{b,f}	29.0 ± 11.5	22
	+	3.17 ± 0.71^{d,f}	38.3 ± 17.8	20
GFP-Stat3βΔ	−	1.42 ± 0.40^{c,g}	27.4 ± 9.9^{h}	42
	+	2.89 ± 0.67^{e,g}	39.1 ± 15.6^{h}	38

$^{a-h}$ For values with identical letter footnotes, $p < 0.05$.

DISCUSSION

Although much has been learned regarding the molecular and cellular biology of Stat3 in the past 15 years, more remains to be discovered regarding its intracellular trafficking and intranuclear dynamics, especially whether or not these features differ between isoforms and the domains within each responsible for any differences observed. Several studies examining intracellular trafficking of Stat3α have been reported (30–38, 42). Fluorescent microscopic studies of cells stained with antibody or expressing Stat3α tagged with GFP or its variants have demonstrated localization of Stat3α within the cytoplasm as well as the nucleus in a diffuse pattern within resting cells (34–39), similar to our findings with GFP-Stat3α. Basal co-localization has been attributed to constitutive shuttling of Stat3α between the cytoplasm and nucleus. Basal shuttling of Stat3α into the nucleus has been attributed to interaction between residues 150 and 162 within the coiled-coil domain with importin-α3 (40). Basal shuttling of Stat3α out of the nucleus mapped to two nuclear export sequences, one contained within residues 404–414 within the DNA-binding domain and the other within residues 524–535 of the linker domain; basal shuttling of Stat3α out of the nucleus is blocked by the CRM1 (chromosome region maintenance 1) inhibitor leptomycin B (36). Early cell fractionation studies (reviewed in Ref. 1) and most studies using fluorescent microscopic imaging (30, 34,

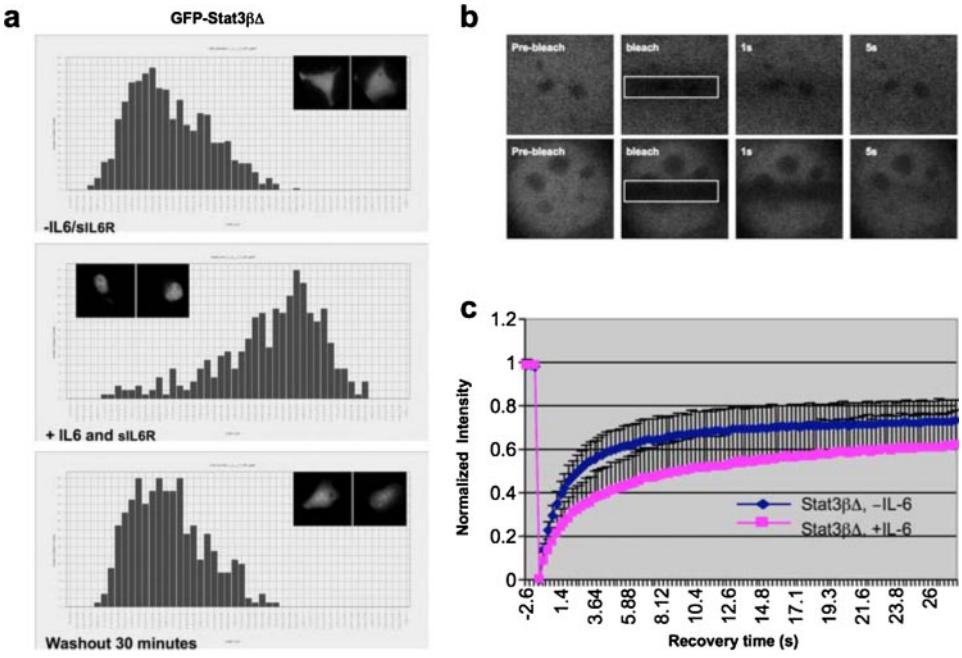

FIGURE 5. **HTM and FRAP analysis of MEF/GFP-Stat3βΔ cells.** *a*, cells were incubated without or with IL-6 (200 ng/ml) and sIL-6R (250 ng/ml) followed by IL-6/sIL-6R washout and incubation in medium alone for the time indicated. Cells were examined by HTM and assayed for FLIN. Histograms show number of cells with FLIN values ranging from 0 to 1.0 in increments of 0.02. Representative fluorescent micrographs of cells are shown in the *inserts*. *b*, representative images showing a single *z* section obtained before photobleaching (*Pre-bleach*), at the end of photobleaching (*bleach*), and at the indicated time points after photobleaching. The *white rectangle* represents the area bleached within the nucleus. *c*, representative recovery curves obtained from FRAP analysis of cells are shown. The initial fluorescence for each cell was assigned a value of 1; fluorescence immediately after bleach was assigned a value of 0. Data shown are the mean ± S.D. of 38–42 cells. Each experiment was repeated at least three times with similar results.

36–38, 41, 42), including those reported herein, have demonstrated accumulation of Stat3α in the nucleus with ligand stimulation. Ligand-mediated nuclear accumulation has been attributed to reduced nuclear export (30) and to interaction of Stat3α arginine residues 214 and 215 in the coiled-coil domain with importin-α5 and, to a lesser extent, importin-α7 (30, 40, 42). Most groups, including ours, have reported that Stat3α is distributed diffusely within the nucleus, excluding the nucleolus, in ligand-stimulated cells, although Herrmann *et al.* (37) described Stat3α within nuclear bodies (0.2–1 μm in size; 10–70 nuclear bodies/nucleus) distinct from splicing factor compartments and promyelocytic leukemia nuclear bodies. Reaccumulation of Stat3α in the cytoplasm after ligand stimulation was blocked by leptomycin B and was attributed to a nuclear export signal sequence located within the C-terminal portion of the coiled-coil domain at residues 306–318 (36). A more recent report suggested that Arg^{214} and Arg^{215} of Stat3α inhibited the interaction between Stat3α and CRM1 (38), since mutation of these residues to alanine increased binding of CRM1 and nuclear export.

One group has previously reported the results of FRAP studies of Stat3α (37) within the nucleoplasm of resting HepG2 and COS-7 cells transiently transfected with Stat3-YFP and within nuclear bodies of ligand-stimulated cells. Whereas they did not report times to half-maximal recovery of fluorescence, they observed a smaller immobile fraction (~23%) in the nucleoplasm of resting cells compared with the immobile fraction with nuclear bodies of ligand-stimulated cells (~49%); FRAP of Stat3α within the nucleoplasm of stimulated cells was not reported. We did not observe nuclear bodies in our studies in either stably transfected MEF cells or transiently transfected HEK293T cells perhaps because we were especially careful to avoid cells with excess overexpression, which we previously demonstrated can lead to artifacts in localization and mobility (26, 31).

Ours is the first report to examine intracellular trafficking and nuclear dynamics of Stat3β and to compare these findings with Stat3α. Similar to GFP-Stat3α, GFP-Stat3β was localized to both the cytoplasm and nucleus with a diffuse distribution in resting HEK293T and MEF cells. GFP-Stat3β also exhibited FLIN similar to GFP-Stat3α. Cytokine stimulation revealed kinetics and cytokine concentration dependence of nuclear accumulation for GFP-Stat3β similar to GFP-Stat3α; the distribution of GFP-Stat3β also was similar to GFP-Stat3α being distributed in a diffuse pattern within the nucleus and excluded from the nucleolus. However, although cytoplasmic reaccumulation was rapid for GFP-Stat3α ($t_{½}$ = 15 min), it was markedly delayed for GFP-Stat3β ($t_{½} > 3$ h). In addition, the intranuclear mobility of the GFP-Stat3β in unstimulated cells was slower than GFP-Stat3α without stimulation. Also, in contrast to Stat3α, Stat3β was slowed further following ligand simulation. Ligand-mediated changes in the immobile fraction were consistent with ligand-mediated changes in intranuclear mobility. Deletion of the unique CT7 domain eliminated prolonged nuclear retention of Stat3β; however, it did not change its intranuclear mobility or percentage immobile fraction.

Studies to determine the mechanism through which the CT7 domain mediates prolonged nuclear retention of Stat3β are under way. Thus far, BLAST analysis (43) did not reveal the presence of a similar amino acid sequence in any nuclear protein in the protein data base, suggesting that the mechanism of CT7-mediated Stat3β nuclear retention may be unique. Also, the addition of the CT7 domain to the C terminus of GFP-Stat3α to generate GFP-Stat3αβ did not result in its prolonged nuclear retention following transient transfection of HEK293T cells (data not shown), indicating that nuclear retention by the CT7 domain is context-dependent.

Although nuclear export of Stat1 appears to be linked to dephosphorylation (44), results with Stat3 are less clear (36, 38). To examine whether or not differences in Stat3 dephosphorylation correlated to differences in nuclear export, we transiently transfected HEK293T cells with each GFP-tagged Stat3 construct and examined cells for cytoplasmic-to-nuclear and nuclear-to-cytoplasmic translocation. Each construct behaved in a manner similar to stably transfected MEF cells (supplemental Fig. 1). Each GFP-tagged Stat3 construct translocated to the nucleus within 30 min following ligand stimulation; although Stat3α and Stat3βΔ recycled to the cytoplasm within 120 min, Stat3β did not. Immunoblotting of whole cell extracts from each revealed no differences in Tyr^{705} phosphorylation status, indicating that the differences in nuclear retention observed did not correlate to Tyr^{705} phosphorylation status.

When phosphorylated on Tyr^{705} to equivalent degrees, Stat3β binds DNA with 20–50-fold more avidity than Stat3α *in vitro* (27) and with 10–20 times more avidity *in vivo* (28). Previous FRAP studies of Stat1 have demonstrated that a Stat1 mutant with enhanced DNA binding also demonstrated reduced mobility compared with wild-type Stat1 (45). These results together with our studies demonstrating that GFP-Stat3βΔ binds DNA with avidity similar to GFP-Stat3β and retains the mobility features of GFP-Stat3β suggest that the distinct nuclear mobility features of Stat3β are the result of its increase DNA binding avidity. Attempts to generate MEF cells stably expressing GFP-tagged Stat3β mutated to decrease DNA binding (GFP-Stat3βDm1 and GFP-Stat3βDm2) were unsuccessful, perhaps due to protein misfolding and degradation (see Fig. 1*c*) resulting in toxicity. However, transient transfection into HeLa cells revealed impaired ligand-stimulated nuclear accumulation of GFP-Stat3βDm2 (Fig. 6). Ligand-induced DNA binding has previously been demonstrated to control nuclear accumulation of Stat1 along with its nuclear mobility (45).

Stat3α and Stat3β demonstrate both distinct and overlapping functions in gene transcription (6, 46–48), normal biology, and pathophysiology. The finding of prolonged nuclear retention may help explain some of these observations. Examination of mice deficient in Stat3β or expressing only Stat3β (49, 50) revealed that Stat3β protected against necrosis of renal tubules, thymus, and liver in the late (>96 h) phase of endotoxemia, down-modulated a subset of endotoxin-inducible genes in the liver, and protected mice from embryonic lethality observed at 6.5–7 days in mice deficient in both Stat3 isoforms (51). Stat3 activation contributes to oncogenesis in many tumor cell systems (52, 53) and has attracted considerable attention as a target for cancer therapy (54–56). Stat3α is the oncogenic isoform, since a constitutively active form of Stat3α alone was

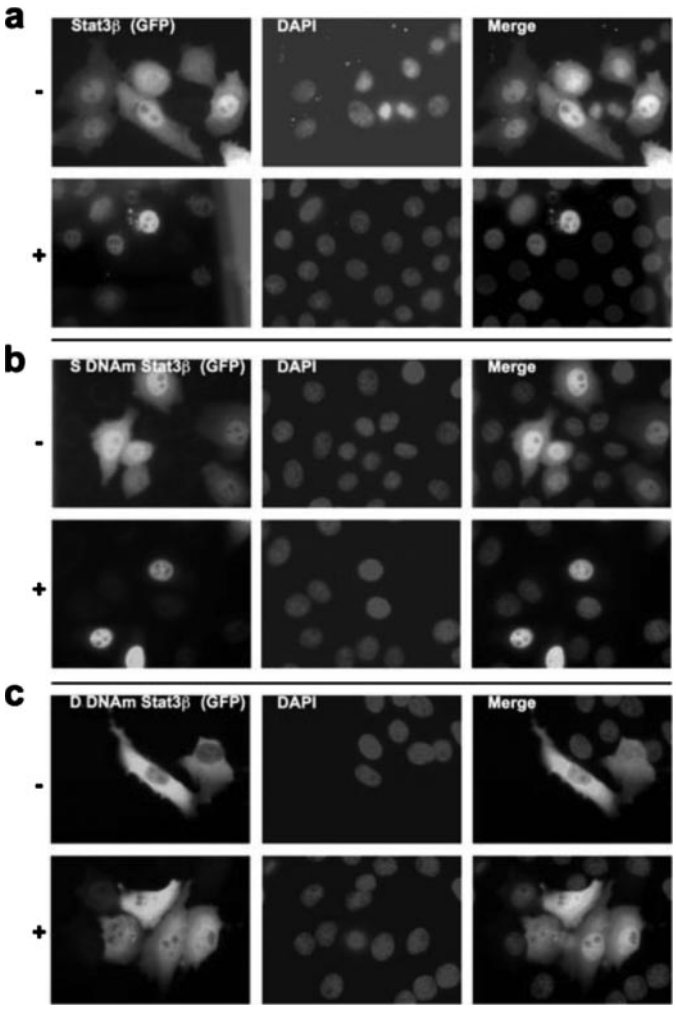

FIGURE 6. **Fluorescence microscope images of HeLa cells transiently transfected with GFP-Stat3β (*a*), GFP-Stat3β Dm1 (*b*), or GFP-Stat3β Dm2 (*c*).** Representative GFP, 4′,6-diamidino-2-phenylindole, and merged images are shown of cells incubated without (−) or with (+) IL-6 (200 ng/ml) and sIL-6R (250 ng/ml).

capable of inducing NIH-3T3 to form foci that formed tumors in nude mice (57), whereas Stat3β antagonized the oncogenic activity of Stat3α (58, 59) downstream of v-Src. It is tempting to speculate that the late protection in endotoxemia, the protection from embryonic lethality and/or the anti-oncogenic effect of Stat3β may be attributable to CT7-mediated prolonged nuclear retention of Stat3β alone or heterodimerized with other STAT protein, such as Stat5A, Stat5B, or Stat1. Last, Stat3 is the most pleiotropic member of the STAT protein family. Our finding that only Stat3β among β isoforms of STAT family members contains a functional domain distinct from its α counterpart may help explain this.

REFERENCES

1. Darnell, J. E., Jr., Kerr, I. M., and Stark, G. R. (1994) *Science* **264,** 1415–1421
2. Wegenka, U. M., Buschmann, J., Lutticken, C., Heinrich, P. C., and Horn, F. (1993) *Mol. Cell. Biol.* **13,** 276–288
3. Akira, S., Nishio, Y., Inoue, M., Wang, X. J., Wei, S., Matsusaka, T., Yoshida, K., Sudo, T., Naruto, M., and Kishimoto, T. (1994) *Cell* **77,** 63–71
4. Zhong, Z., Wen, Z., and Darnell, J. E., Jr. (1994) *Science* **264,** 95–98
5. Shuai, K., Stark, G. R., Kerr, I. M., and Darnell, J. E., Jr. (1993) *Science* **261,** 1744–1746
6. Schaefer, T. S., Sanders, L. K., and Nathans, D. (1995) *Proc. Natl. Acad. Sci. U. S. A.* **92,** 9097–9101
7. Chakraborty, A., White, S. M., Schaefer, T. S., Ball, E. D., Dyer, K. F., and Tweardy, D. J. (1996) *Blood* **88,** 2442–2449
8. Caldenhoven, E., van Dijk, T. B., Solari, R., Armstrong, J., Raaijmakers, J. A., Lammers, J. W., Koenderman, L., and de Groot, R. P. (1996) *J. Biol. Chem.* **271,** 13221–13227
9. Hoey, T., Zhang, S., Schmidt, N., Yu, Q., Ramchandani, S., Xu, X., Naeger, L. K., Sun, Y. L., and Kaplan, M. H. (2003) *EMBO J.* **22,** 4237–4248
10. Wang, D., Stravopodis, D., Teglund, S., Kitazawa, J., and Ihle, J. N. (1996) *Mol. Cell. Biol.* **16,** 6141–6148
11. Ripperger, J. A., Fritz, S., Richter, K., Hocke, G. M., Lottspeich, F., and Fey, G. H. (1995) *J. Biol. Chem.* **270,** 29998–30006
12. Patel, B. K., Pierce, J. H., and LaRochelle, W. J. (1998) *Proc. Natl. Acad. Sci. U. S. A.* **95,** 172–177
13. Sherman, M. A., Powell, D. R., and Brown, M. A. (2002) *J. Immunol.* **169,** 3811–3818
14. Azam, M., Lee, C., Strehlow, I., and Schindler, C. (1997) *Immunity* **6,** 691–701
15. Chakraborty, A., and Tweardy, D. J. (1998) *J. Leukocyte Biol.* **64,** 675–680
16. Lokuta, M. A., McDowell, M. A., and Paulnock, D. M. (1998) *J. Immunol.* **161,** 1594–1597
17. Caldenhoven, E., van Dijk, T. B., Raaijmakers, J. A., Lammers, J. W., Koenderman, L., and de Groot, R. P. (1999) *Mol. Cell. Biol. Res Commun.* **1,** 95–101
18. Ilaria, R. L., Jr., Hawley, R. G., and Van Etten, R. A. (1999) *Blood* **93,** 4154–4166
19. Sherman, M. A., Secor, V. H., and Brown, M. A. (1999) *J. Immunol.* **162,** 2703–2708
20. Piazza, F., Valens, J., Lagasse, E., and Schindler, C. (2000) *Blood* **96,** 1358–1365
21. Costa-Pereira, A. P., Tininini, S., Strobl, B., Alonzi, T., Schlaak, J. F., Is'harc, H., Gesualdo, I., Newman, S. J., Kerr, I. M., and Poli, V. (2002) *Proc. Natl. Acad. Sci. U. S. A.* **99,** 8043–8047
22. Shao, H., Xu, X., Jing, N., and Tweardy, D. J. (2006) *J. Immunol.* **176,** 2933–2941
23. Dong, S., and Tweardy, D. J. (2002) *Blood* **99,** 2637–2646
24. Marcelli, M., Stenoien, D. L., Szafran, A. T., Simeoni, S., Agoulnik, I. U., Weigel, N. L., Moran, T., Mikic, I., Price, J. H., and Mancini, M. A. (2006) *J. Cell. Biochem.* **98,** 770–788
25. Berno, V., Hinojos, C. A., Amazit, L., Szafran, A. T., and Mancini, M. A. (2006) *Methods Enzymol.* **414,** 188–210
26. Dong, S., Stenoien, D. L., Qiu, J., Mancini, M. A., and Tweardy, D. J. (2004) *Mol. Cell. Biol.* **24,** 4465–4475
27. Park, O. K., Schaefer, T. S., and Nathans, D. (1996) *Proc. Natl. Acad. Sci. U. S. A.* **93,** 13704–13708
28. Schaefer, T. S., Sanders, L. K., Park, O. K., and Nathans, D. (1997) *Mol. Cell. Biol.* **17,** 5307–5316
29. Sasse, J., Hemmann, U., Schwartz, C., Schniertshauer, U., Heesel, B., Landgraf, C., Schneider-Mergener, J., Heinrich, P. C., and Horn, F. (1997) *Mol. Cell. Biol.* **17,** 4677–4686
30. Pranada, A. L., Metz, S., Herrmann, A., Heinrich, P. C., and Muller-Newen, G. (2004) *J. Biol. Chem.* **279,** 15114–15123
31. Stenoien, D. L., Patel, K., Mancini, M. G., Dutertre, M., Smith, C. L., O'Malley, B. W., and Mancini, M. A. (2001) *Nat. Cell Biol.* **3,** 15–23
32. Lippincott-Schwartz, J., Altan-Bonnet, N., and Patterson, G. H. (2003) *Nat. Cell Biol.* **17,** (suppl.) 7–14
33. Park, O. K., Schaefer, L. K., Wang, W., and Schaefer, T. S. (2000) *J. Biol. Chem.* **275,** 32244–32249
34. Kretzschmar, A. K., Dinger, M. C., Henze, C., Brocke-Heidrich, K., and Horn, F. (2004) *Biochem. J.* **377,** 289–297
35. Meyer, T., Gavenis, K., and Vinkemeier, U. (2002) *Exp. Cell Res.* **272,** 45–55
36. Bhattacharya, S., and Schindler, C. (2003) *J. Clin. Invest.* **111,** 553–559
37. Herrmann, A., Sommer, U., Pranada, A. L., Giese, B., Kuster, A., Haan, S., Becker, W., Heinrich, P. C., and Muller-Newen, G. (2004) *J. Cell Sci.* **117,** 339–349
38. Sato, N., Tsuruma, R., Imoto, S., Sekine, Y., Muromoto, R., Sugiyama, K., and Matsuda, T. (2005) *Biochem. Biophys. Res. Commun.* **336,** 617–624

39. Reich, N. C., and Liu, L. (2006) *Nat. Rev. Immunol.* **6,** 602–612
40. Liu, L., McBride, K. M., and Reich, N. C. (2005) *Proc. Natl. Acad. Sci. U. S. A.* **102,** 8150–8155
41. Sato, N., Kawai, T., Sugiyama, K., Muromoto, R., Imoto, S., Sekine, Y., Ishida, M., Akira, S., and Matsuda, T. (2005) *Int. Immunol.* **17,** 1543–1552
42. Ma, J., and Cao, X. (2006) *Cell Signal* **18,** 1117–1126
43. Altschul, S. F., Madden, T. L., Schaffer, A. A., Zhang, J., Zhang, Z., Miller, W., and Lipman, D. J. (1997) *Nucleic Acids Res.* **25,** 3389–3402
44. Haspel, R. L., and Darnell, J. E., Jr. (1999) *Proc. Natl. Acad. Sci. U. S. A.* **96,** 10188–10193
45. Meyer, T., Marg, A., Lemke, P., Wiesner, B., and Vinkemeier, U. (2003) *Genes Dev.* **17,** 1992–2005
46. Zhang, X., Wrzeszczynska, M. H., Horvath, C. M., and Darnell, J. E., Jr. (1999) *Mol. Cell. Biol.* **19,** 7138–7146
47. Yoo, J. Y., Wang, W., Desiderio, S., and Nathans, D. (2001) *J. Biol. Chem.* **276,** 26421–26429
48. Zhang, X., and Darnell, J. E., Jr. (2001) *J. Biol. Chem.* **276,** 33576–33581
49. Yoo, J. Y., Huso, D. L., Nathans, D., and Desiderio, S. (2002) *Cell* **108,** 331–344
50. Maritano, D., Sugrue, M. L., Tininini, S., Dewilde, S., Strobl, B., Fu, X., Murray-Tait, V., Chiarle, R., and Poli, V. (2004) *Nat. Immunol.* **5,** 401–409
51. Takeda, K., Noguchi, K., Shi, W., Tanaka, T., Matsumoto, M., Yoshida, N., Kishimoto, T., and Akira, S. (1997) *Proc. Natl. Acad. Sci. U. S. A.* **94,** 3801–3804
52. Bowman, T., Garcia, R., Turkson, J., and Jove, R. (2000) *Oncogene* **19,** 2474–2488
53. Niu, G., Wright, K. L., Huang, M., Song, L., Haura, E., Turkson, J., Zhang, S., Wang, T., Sinibaldi, D., Coppola, D., Heller, R., Ellis, L. M., Karras, J., Bromberg, J., Pardoll, D., Jove, R., and Yu, H. (2002) *Oncogene* **21,** 2000–2008
54. Turkson, J. (2004) *Expert Opin. Ther. Targets* **8,** 409–422
55. Jing, N., and Tweardy, D. J. (2005) *Anticancer Drugs* **16,** 601–607
56. Darnell, J. E. (2005) *Nat. Med.* **11,** 595–596
57. Bromberg, J. F., Wrzeszczynska, M. H., Devgan, G., Zhao, Y., Pestell, R. G., Albanese, C., and Darnell, J. E., Jr. (1999) *Cell* **98,** 295–303
58. Bromberg, J. F., Horvath, C. M., Besser, D., Lathem, W. W., and Darnell, J. E., Jr. (1998) *Mol. Cell. Biol.* **18,** 2553–2558
59. Turkson, J., Bowman, T., Garcia, R., Caldenhoven, E., De Groot, R. P., and Jove, R. (1998) *Mol. Cell. Biol.* **18,** 2545–2552

Stat3 Isoforms, α and β, Demonstrate Distinct Intracellular Dynamics with Prolonged Nuclear Retention of Stat3 β Mapping to Its Unique C-terminal End

Ying Huang, Jihui Qiu, Shuo Dong, Michele S. Redell, Valeria Poli, Michael A. Mancini and David J. Tweardy

J. Biol. Chem. 2007, 282:34958-34967.
doi: 10.1074/jbc.M704548200 originally published online September 12, 2007
